25 Copies

NASA TECHNICAL MEMORANDUM

NASA TM X-52285

NASA TM X-52285

INVESTIGATION OF A SUBMERGED NOZZLE FOR SOLID ROCKETS

by Reino J. Salmi and James J. Pelouch Jr.
Lewis Research Center
Cleveland, Ohio

TECHNICAL PAPER proposed for presentation at Second Solid Propulsion Conference sponsored by the American Institute of Aeronautics and Astronautics and the Interagency Chemical Rocket Propulsion Group
Anaheim, California, June 6-8, 1967

NATIONAL AERONAUTICS AND SPACE ADMINISTRATION · WASHINGTON, D.C. · 1967

E-3779

INVESTIGATION OF A SUBMERGED NOZZLE FOR SOLID ROCKETS

by Reino J. Salmi and James J. Pelouch Jr.

Lewis Research Center
Cleveland, Ohio

TECHNICAL PAPER proposed for presentation at

Second Solid Propulsion Conference
sponsored by the American Institute of Aeronautics and Astronautics
and the Interagency Chemical Rocket Propulsion Group
Anaheim, California, June 6-8, 1967

NATIONAL AERONAUTICS AND SPACE ADMINISTRATION

INVESTIGATION OF A SUBMERGED NOZZLE FOR SOLID ROCKETS

by Reino J. Salmi and James J. Pelouch Jr.

Lewis Research Center
National Aeronautics and Space Administration
Cleveland, Ohio

INTRODUCTION

The provision of thrust vector control for solid rockets is a continuing problem. One of the proposed methods of providing TVC for the 260-inch solid rocket is that of a gimballed nozzle, utilizing a free-standing nozzle which is supported externally by a spherical bearing from the rocket aft-end casing. As shown in the schematic drawing of figure 1, the spherical bearing is located in the region of the nozzle throat, with the convergent section of the convergent-divergent nozzle submerged within the aft-end casing. In addition to providing the feasibility of gimballing, the submerged nozzle is located close to the propellant grain, thereby reducing the overall length of the rocket.

The submerged nozzle will be tested on the 260-inch solid rocket motor (SL-3), which is scheduled for firing in mid-year 1967. For this test, however, the nozzle will not be gimballed and the annular clearance space between the nozzle lip and the aft-end casing, which is necessary for the gimballing action, will be protected by insulating compounds. The SL-3 nozzle was originally designed with the assumption that the flow in the annular channel would be essentially stagnant and not subject to the erosive action of the hot exhaust gases flowing into the nozzle. However, further study of the nozzle created some concern for the validity of this assumption and for the structural integrity of the nozzle. It appeared possible that the hot exhaust gases flowing out of the assymetric grain port could induce pressure unbalances that would cause a circumferential flow of the exhaust gases at high Mach numbers in the annular channel. Figure 2 presents a cutaway isometric drawing that illustrates the possible flow phenomena. The exhaust flow is shown entering the annular channel in the region between the grain lobes, flowing circumferentially in the annular channel behind the nozzle lip and exiting in the region directly behind the grain lobes. It was reasoned that the region directly behind the grain lobes would experience lower pressures due to separation of the exhaust gases from the blunt base. An experimental investigation of the probelm was, therefore, undertaken to determine whether or not it existed and its possible severity.

APPARATUS AND PROCEDURE

Tests to determine the velocity and direction of the exhaust flow in the annular channel were made at the Lewis Research Center with an 0.07-scale model of the 260-inch solid rocket. Compressed air was used to simulate the exhaust gases. The tests were made in two different facilities. The initial tests were made in an altitude test chamber. In these tests, the model chamber pressure was set at 20 psia and the test chamber pressure at 2 psia. Later tests were made in an atmospheric test stand shown in figure 4. The tests here were made with the model chamber pressure set at 30 psia. High pressure air was brought to the annular chamber between the simulated propellant grain and the outer shell through the pipe shown entering the model side towards the closed end.

The flow direction in the annular channel was determined from high-speed movies of the motions of wool tufts attached to the channel walls. A transparent aft-end casing was used to accommodate the visual observations. Figure 5 shows the submerged nozzle which was made of steel. It was cut off just downstream of the throat since the divergent part of the nozzle would have no effect on the entrance region flow. The back side of the nozzle lip which forms one wall of the annular channel was painted white and black tufts were cemented to it. The transparent aft-end casing, which is shown in figure 6, had red tufts attached to it on that part of its surface which formed the other wall of the annular channel. The different colored tufts differentiated between the flows along each wall.

The flow velocities in the annular channel and on the nozzle surface were determined from measurements of the local static and total pressures. One row of orifices was installed in the nozzle and the aft-end nozzle assembly was rotated relative to the simulated propellant grain to obtain circumferential measurements. The pressures were measured with mercury and TBE manometer boards and recorded photographically. The total pressure probes in the annular passage could be rotated remotely to obtain the maximum value. The position of the probe also indicated the direction of the channel flow at that point.

To simulate the emanation of burning gases from the surface of the solid propellant grain, the model grains were fabricated from sheet steel with uniformly spaced 3/16-inch diameter holes. Two of the grains used are shown in figure 7. The total area of the holes was about 40 percent of the nozzle throat area to assure choking of the holes and uniform air distribution. The grain shown on the left is a full grain with flat ends on the lobes. The flat ends slant inward at an angle of 30 degrees from a normal. It is the type of grain that will be tested on the SL-3 motor. The grain shown on the right was used to simulate the condition where the grain has regressed 34 percent due to burning. The grain lobes are considerably smaller and the port area enlarged. A full three-lobe grain with modified lobe ends was also tested. As shown in figure 8, the ends of the grain lobes were shaped like wedges having 90 degree included angles. It was thought that this modification might increase the lobe base pressures and help alleviate the potential circulation problem.

Two nozzle geometries were included in the tests. The first nozzle simulated the initial SL-3 nozzle design. The second nozzle contour, which was finally incorporated into the SL-3 motor, was established on the basis of test on the first nozzle. These modifications will be discussed later. Figure 9 shows a comparison between the initial

model nozzle contour and the initial SL-3 motor. The initial model nozzle did not duplicate exactly the geometry of the initial SL-3 design because of a design error and some modifications to allow more effective tuft observation. These differences should not have a large effect on the results, however.

RESULTS

The results obtained with the first nozzle and the full size flat-ended grain are shown in figure 10. This view assumes a transparent aft-end casing so that the region of recirculation in the annular clearance space between the nozzlelip and the aft-end casing can be seen as the white annular area. The arrows on the left side of the white annulus indicate direction of the flow observed from the tuft movies. As was expected, the exhaust gases entered the annular passage in the region midway between the grain lobes, flowed along the channel and exited in the region directly behind the grain lobes. The flow velocities are shown on the right hand side of the annular passage by the lines of constant Mach number. The highest Mach numbers were slightly greater than 0.2 and occurred near the region directly behind the grain lobes. The minimum values were less than 0.05 and they occurred in the area midway between the grain lobes. The effects of modifying the grain lobe ends to the wedge shape are presented in figure 11. The modification had only a slight effect on the highest Mach numbers in the region behind the grain lobes but the low Mach number region extended over a much wider area. The same general flow direction pattern was observed as with the flat ended grain. Figure 12 presents the results obtained with the 34 percent regressed grain which simulated the effects of grain consumption due to burning. The flow pattern in the passage appeared the same as with the full grains but it seemed more turbulent. The flow Mach numbers were considerably reduced, however. A favorable effect of grain burning is, therefore, indicated.

As a result of the exhaust flow patterns and Mach numbers observed from the tests of the first nozzle, modifications were made to the design of the SL-3 nozzle. These modifications are shown in figure 13. Additional Pban insulation was used to fill the narrow bottom valley of the channel. The silica overwrap next to the steel was extended farther up the back side of the lip and the ablative material in one region was changed from silica tape to carbon phenolic tape.

The results obtained with the new nozzle contour, which conformed closely to the modified SL-3 nozzle, and with the full grain with flat ends are presented in figure 14. The results indicated that the flow Mach numbers were considerably lower than those obtained with the original nozzle and the same grain. The flow patterns were in general similar to those with the first nozzle. With the increased protection against erosion and the lower channel flow velocities indicated by the results with the new nozzle, the SL-3 nozzle should withstand the firing as far as erosion in the annular channel is concerned. The results with the 34-percent regressed grain are presented in figure 15 and show further reductions in the flow velocities. It is probable that by the time the grain has eroded 50 percent the circumferential flow in the annular passage will be virtually eliminated.

In addition to its effects on the flow in the annular channel, the assymetric grain port will also distort the flow in the nozzle, with possible reductions in the flow coefficient and uneven erosion of the ablative surfaces. The circumferential Mach number variations for two nozzle stations are presented in figure 16. With the 100-percent grain there was relatively little circumferential Mach number variation at station 1 near the nozzle throat (figure 13) whereas at a station 3, upstream in the entrance region, lower Mach numbers ocurred in the region directly behind the grain than at the point midway between the grain lobes. With the 34-percent regressed grain, however, there was very little distortion at either nozzle station. The Mach number variations indicated by figure 16 do not present any serious performance deficiencies, however, and any uneven erosion in the lower Mach number regions of the nozzle would tend to disappear as the grain burning progresses.

SUMMARY OF RESULTS

Tests of an 0.07-scale compressed-air model of the 260-inch solid rocket with a submerged nozzle indicated that the assymetric grain port shape induced a circumferential flow in the annular passage between the submerged nozzle lip and the aft-end casing. Subsequent modifications to the SL-3 nozzle to provide increased insulation against the erosive effects of the hot exhaust gases in the annular channel also reduced the flow velocities in the channel. Simulated erosion of the grain due to burning also greatly reduced the flow velocities in this area. Some distortion of the flow in the nozzle was also observed particularly with the 100-percent grain.

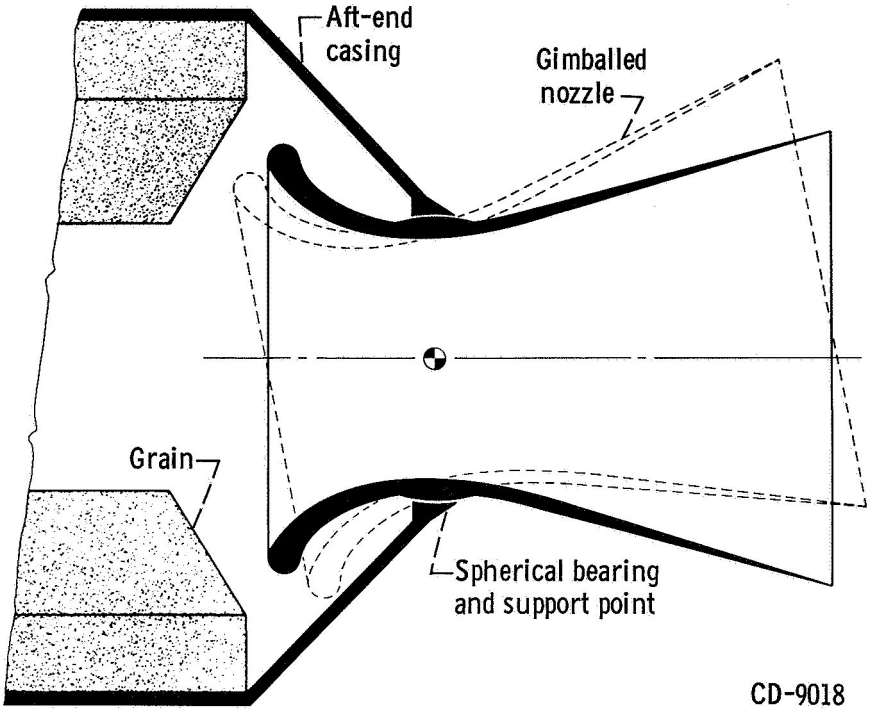

Figure 1. - Submerged nozzle concept.

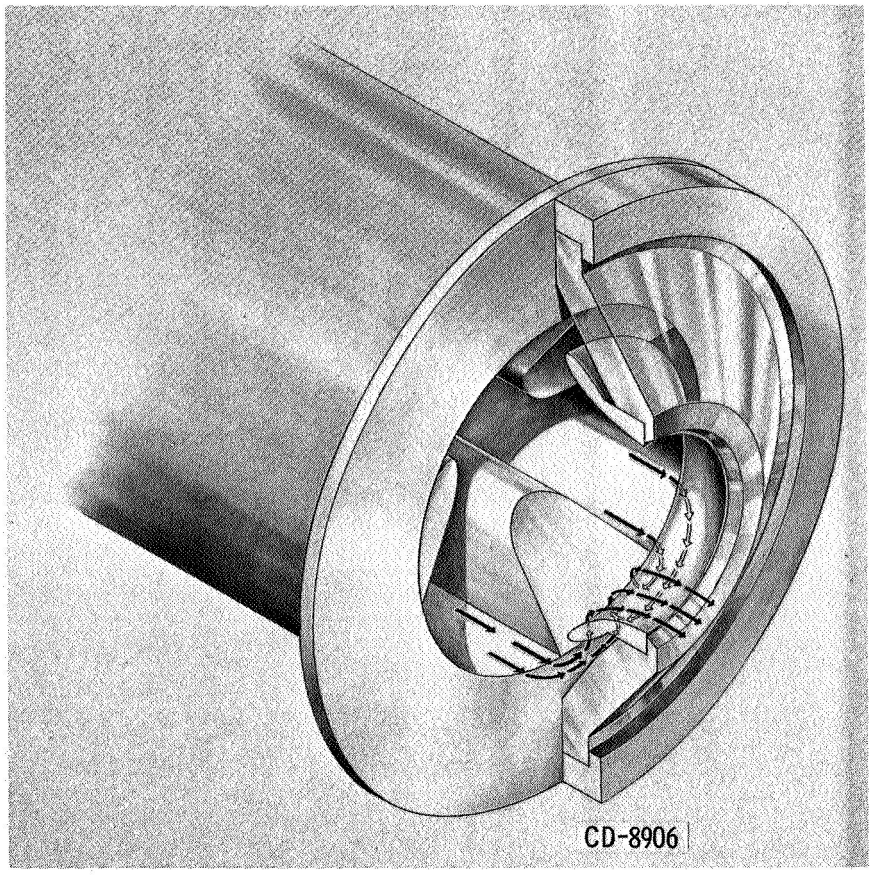

Figure 2. - Possible flow pattern in SL-3 motor.

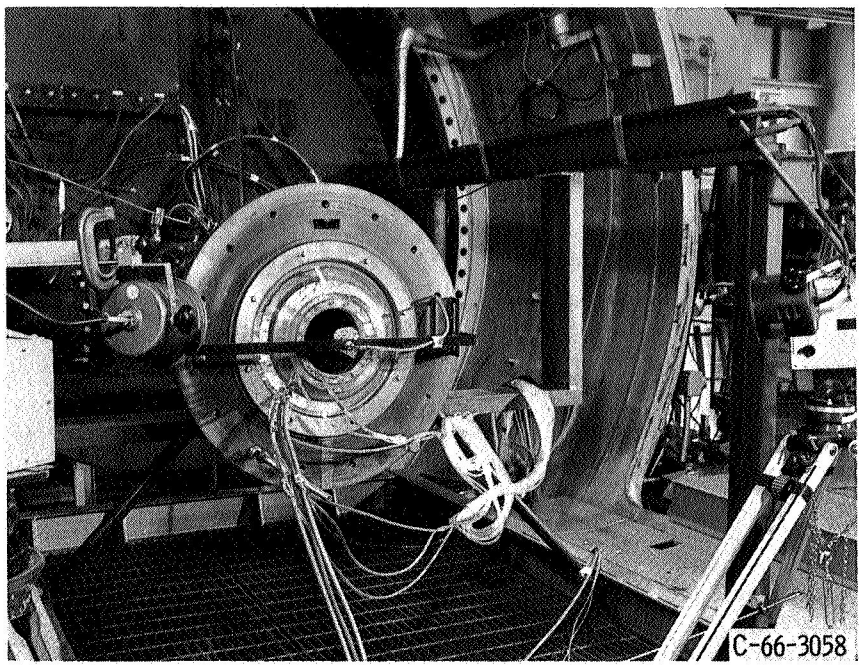

Figure 3. - Model test setup in altitude chamber.

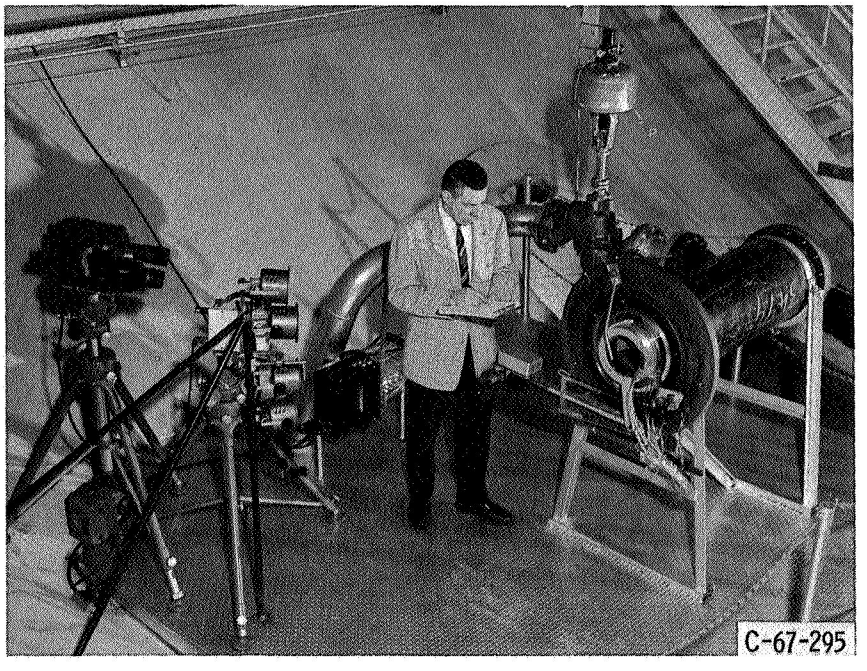

Figure 4. - Model setup in atmospheric test facility.

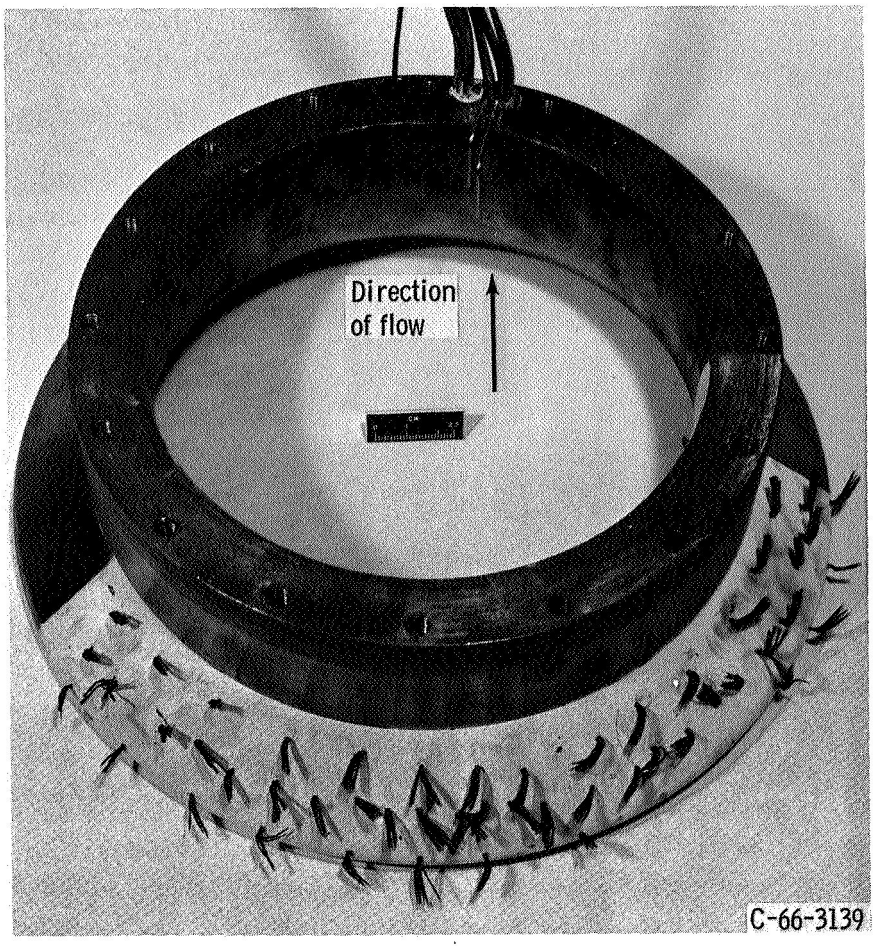

Figure 5. - Model nozzle I.

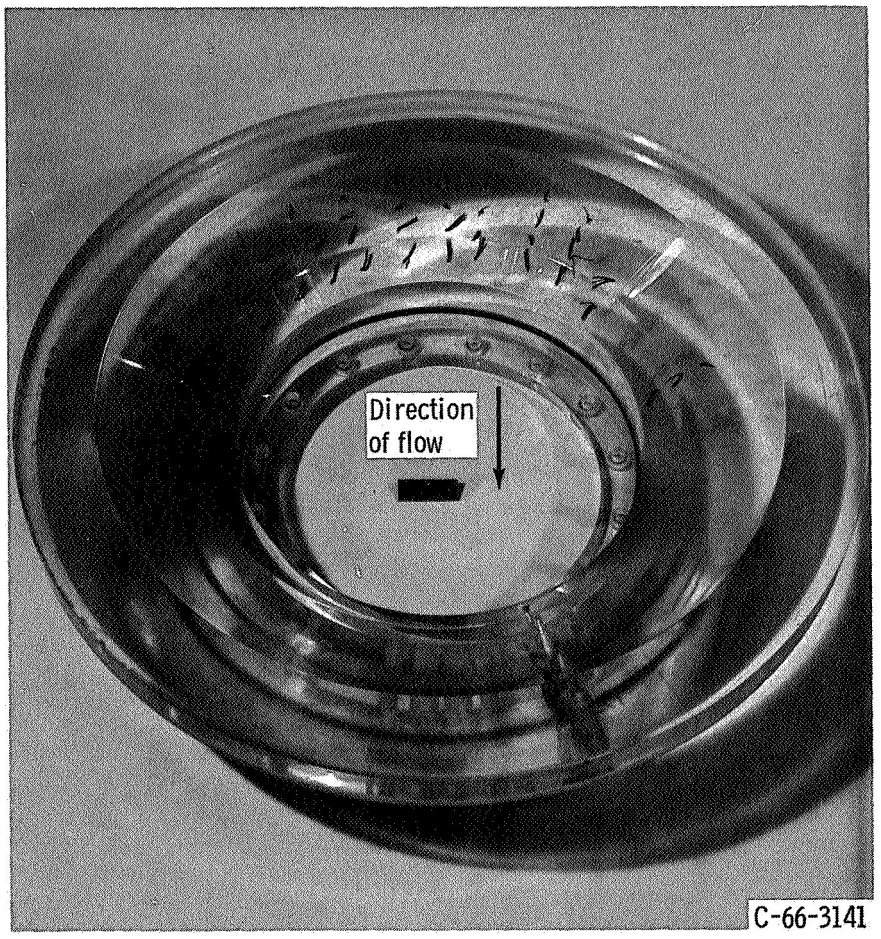

Figure 6. - Model transparent aft-end casing.

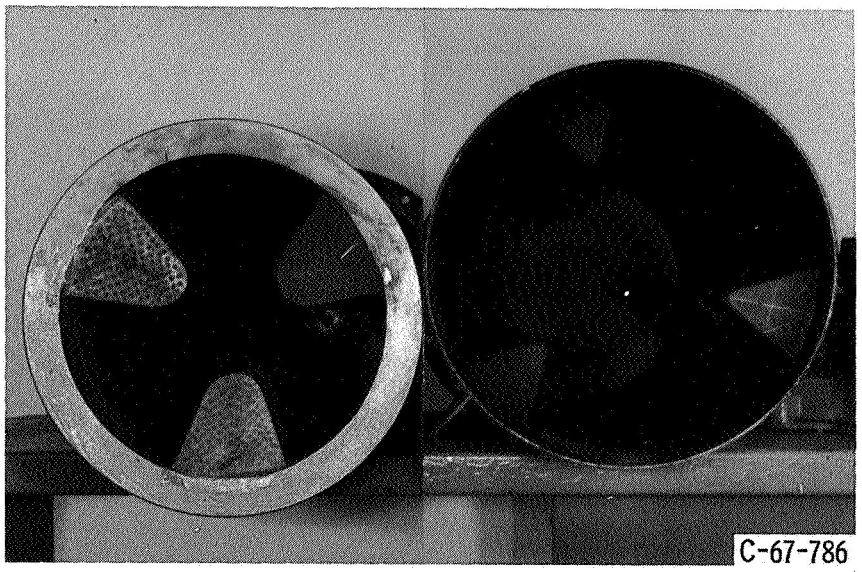

100% Grain flat lobe ends

34% Regressed grain flat lobe ends

Figure 7. - Simulated propellant grains.

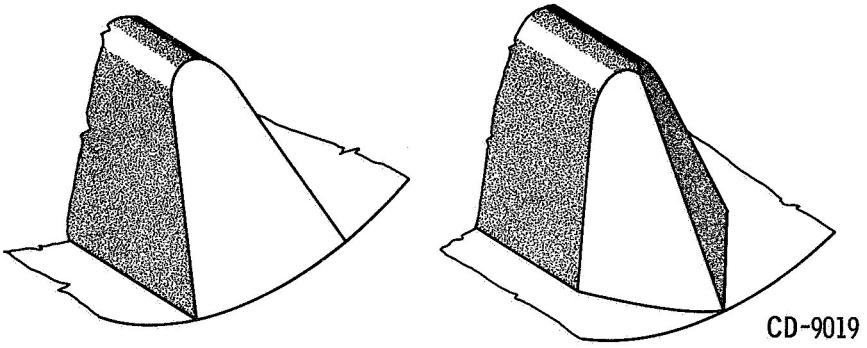

Flat end grain lobe

90° Wedge end grain lobe

Figure 8. - Grain lobe end modification.

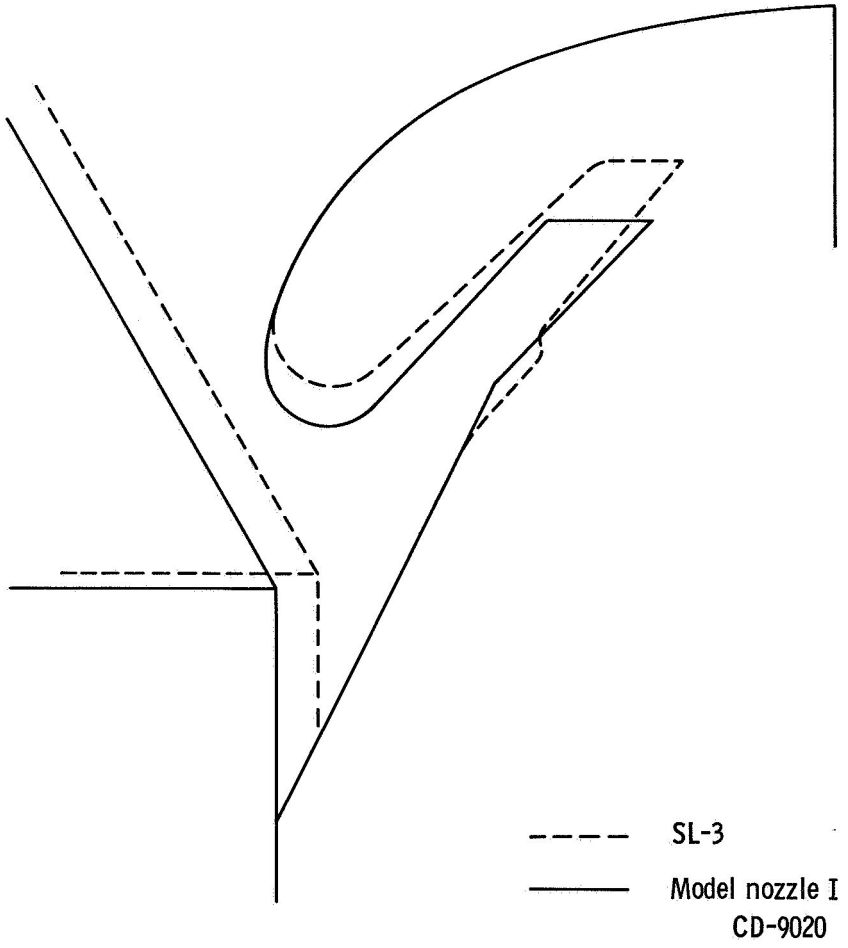

Figure 9. - Comparison of SL-3 and model nozzle I contour.

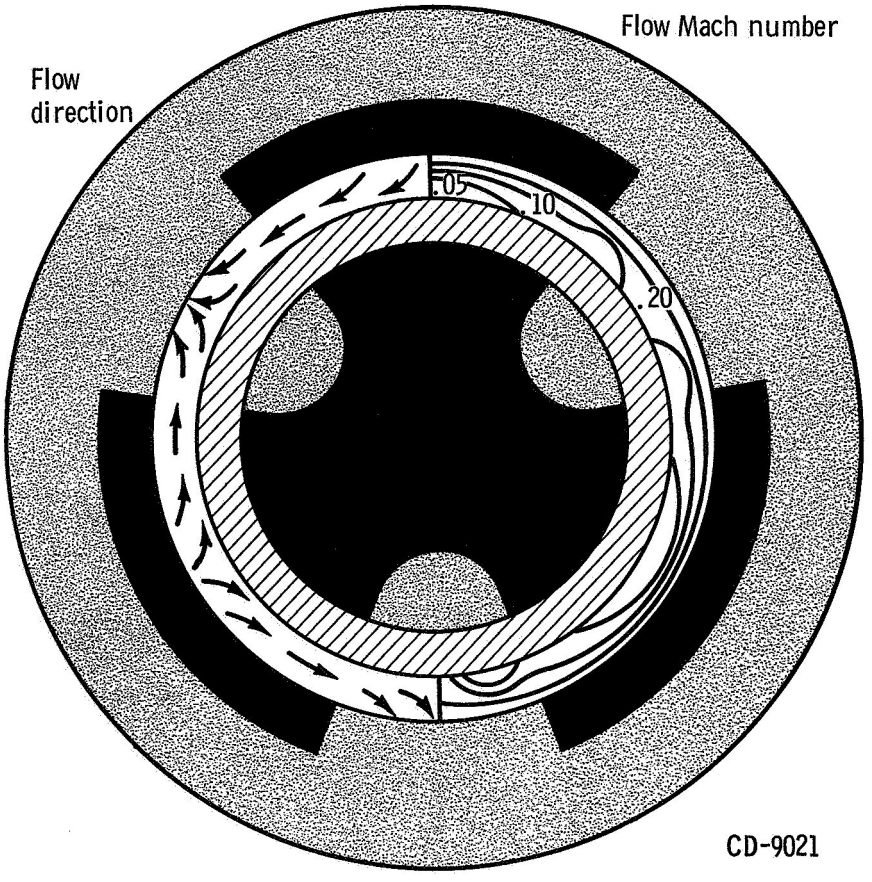

Figure 10. - Annular channel flow characteristics, 100% grain, flat lobe ends, nozzle I.

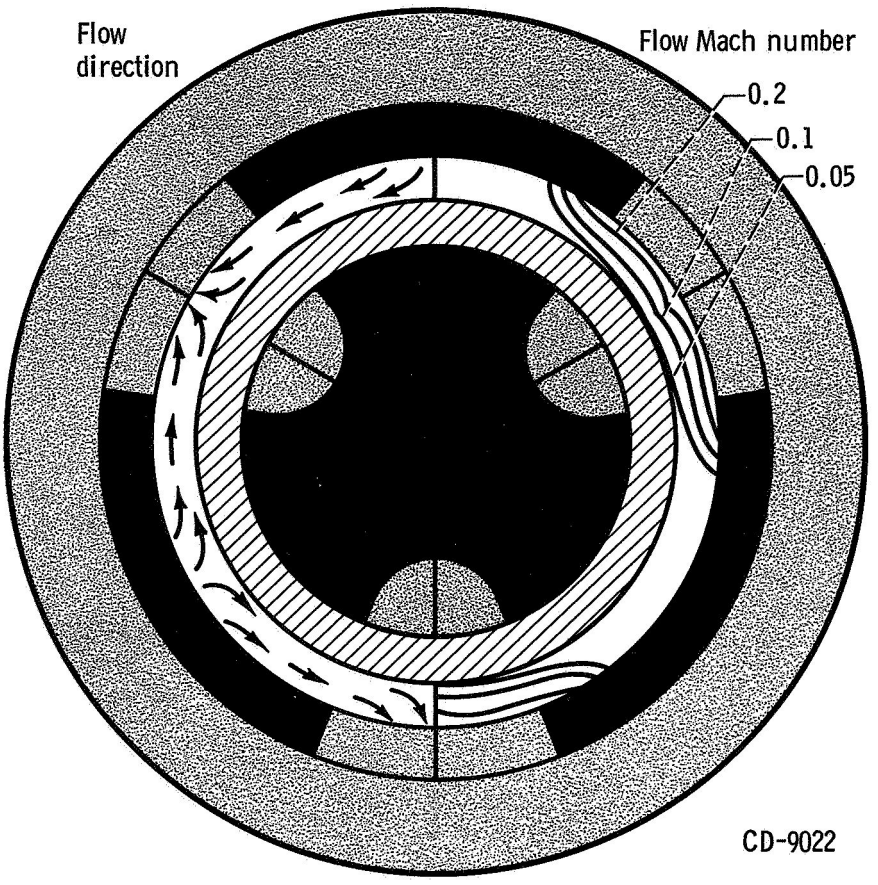

Figure 11. - Annular channel flow characteristics, 100% grain, 90° wedge lobe ends, nozzle I.

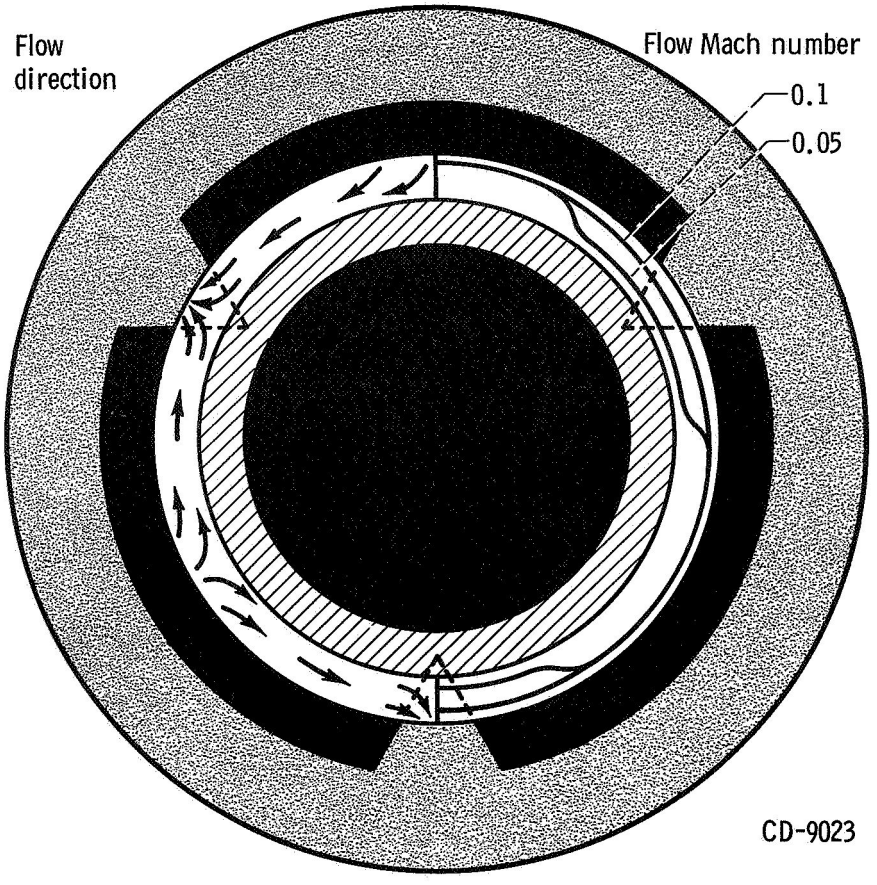

Figure 12. - Annular channel flow characteristics, 34% regressed grain, nozzle I.

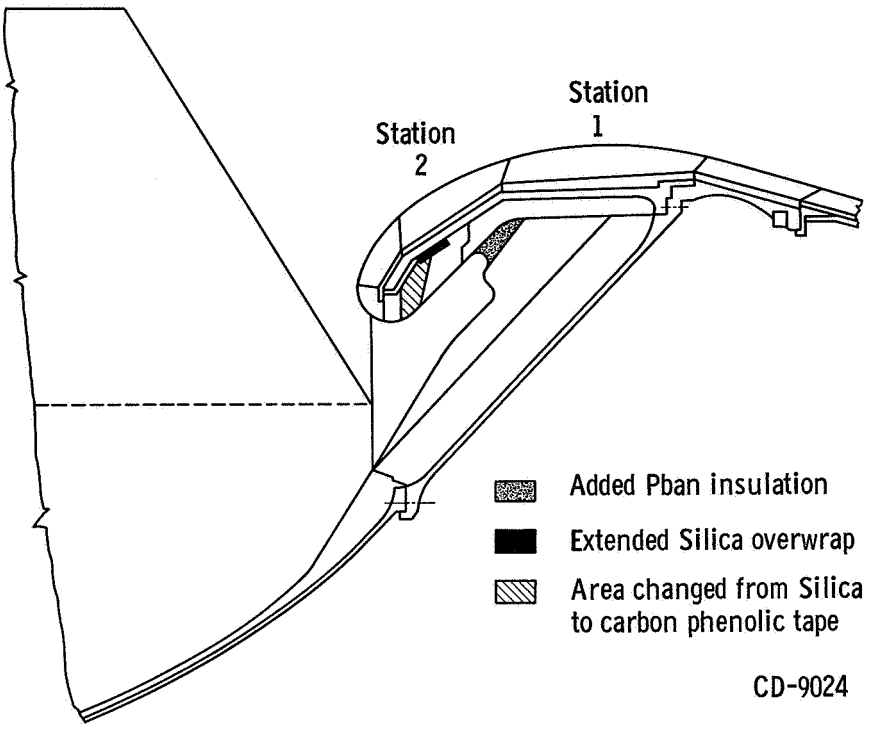

Figure 13. - Modifications to SL-3 nozzle.

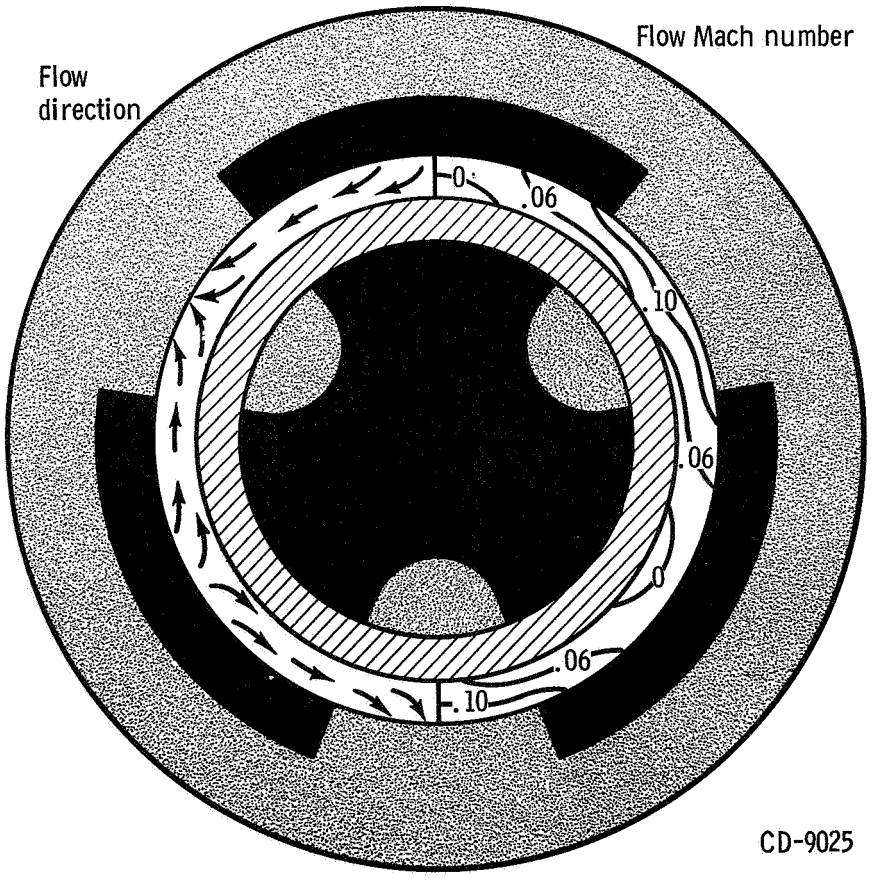

Figure 14. - Annular channel flow characteristics, 100% grain, flat ends, nozzle II.

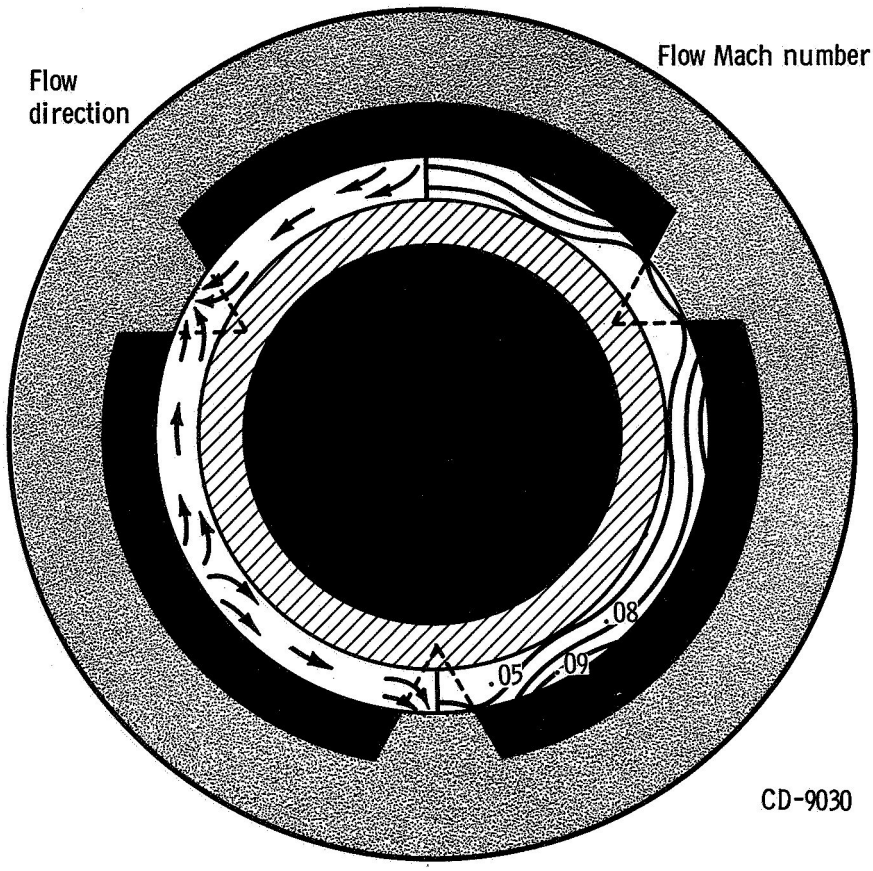

Figure 15. - Annular channel flow characteristics, 34%-regressed grain, nozzle II.

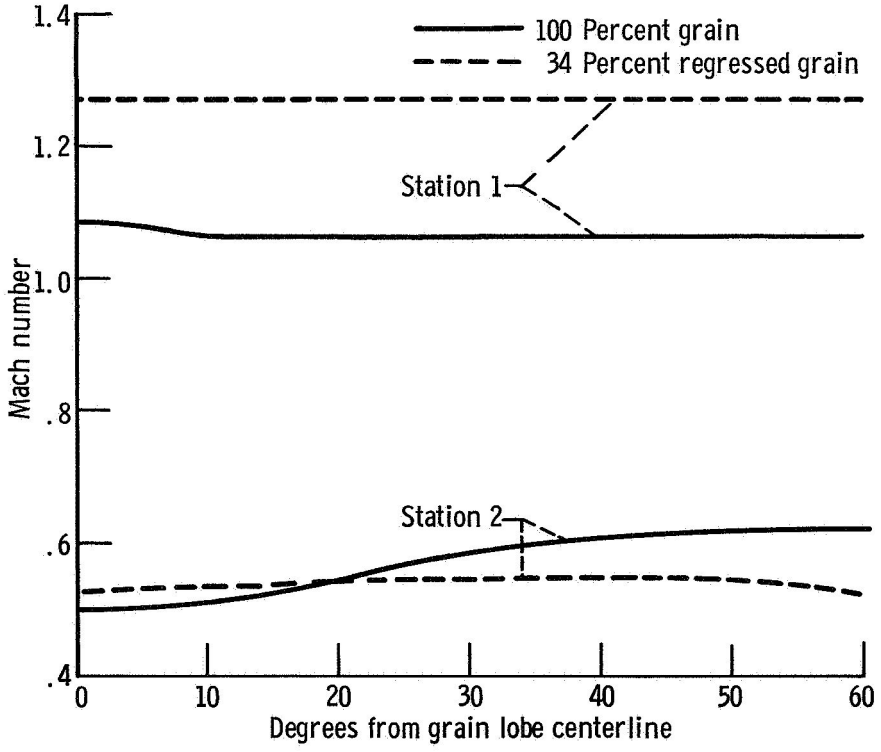

Figure 16. - Nozzle flow distortion due to assymetric grain port.